AGU PUBLICATIONS

JGR

Journal of Geophysical Research: Space Physics

RESEARCH ARTICLE
10.1002/2014JA020360

Key Points:
- We show full local time coverage of the equatorial electric field from THEMIS
- Local maximum occurs near $L = 4$ during active times in dawn and dusk sectors
- No clear increased electric field with K_p near midnight at high L

Correspondence to:
S. Califf,
califf@colorado.edu

Citation:
Califf, S., et al. (2014), THEMIS measurements of quasi-static electric fields in the inner magnetosphere, *J. Geophys. Res. Space Physics*, *119*, 9939–9951, doi:10.1002/2014JA020360.

Received 8 JUL 2014
Accepted 22 OCT 2014
Accepted article online 28 OCT 2014
Published online 18 DEC 2014

THEMIS measurements of quasi-static electric fields in the inner magnetosphere

S. Califf[1], X. Li[1], L. Blum[1], A. Jaynes[1], Q. Schiller[1], H. Zhao[1], D. Malaspina[1], M. Hartinger[2], R. A. Wolf[3], D. E. Rowland[4], J. R. Wygant[5], and J. W. Bonnell[6]

[1]Laboratory for Atmospheric and Space Physics, University of Colorado, Boulder, Colorado, USA, [2]Department of Atmospheric, Oceanic and Space Sciences, University of Michigan, Ann Arbor, Michigan, USA, [3]Department of Physics and Astronomy, Rice University, Houston, Texas, USA, [4]Goddard Space Flight Center, Greenbelt, Maryland, USA, [5]School of Physics and Astronomy, University of Minnesota, Twin Cities, Minneapolis, Minnesota, USA, [6]Space Science Laboratory, University of California, Berkeley, California, USA

Abstract We use 4 years of Time History of Events and Macroscale Interactions during Substorms (THEMIS) double-probe measurements to offer, for the first time, a complete picture of the dawn-dusk electric field covering all local times and radial distances in the inner magnetosphere based on in situ equatorial observations. This study is motivated by the results from the CRRES mission, which revealed a local maximum in the electric field developing near Earth during storm times, rather than the expected enhancement at higher L shells that is shielded near Earth as suggested by the Volland-Stern model. The CRRES observations were limited to the duskside, while THEMIS provides complete local time coverage. We show strong agreement with the CRRES results on the duskside, with a local maximum near $L = 4$ for moderate levels of geomagnetic activity and evidence of strong electric fields inside $L = 3$ during the most active times. The extensive data set from THEMIS also confirms the day/night asymmetry on the duskside, where the enhancement is closest to Earth in the dusk-midnight sector, and is farther away closer to noon. A similar, but smaller in magnitude, local maximum is observed on the dawnside near $L = 4$. The noon sector shows the smallest average electric fields, and for more active times, the enhancement develops near $L = 7$ rather than $L = 4$. We also investigate the impact of the uncertain boom-shorting factor on the results and show that while the absolute magnitude of the electric field may be underestimated, the trends with geomagnetic activity remain intact.

1. Introduction

The quasi-static electric field in the inner magnetosphere drives many processes critical to understanding magnetospheric plasma dynamics. The electric field is set up by the interaction of the solar wind with the Earth's magnetic field, creating a large-scale dawn-to-dusk convection electric field that drives plasma earthward from the magnetotail. Earthward convection transports plasma sheet particles to regions of higher-magnetic field strength, where they are adiabatically energized and contribute to the ring current. Curvature and gradient drifts cause electrons to drift eastward and ions to drift westward, leading to a polarization electric field pointing from dusk to dawn that shields the inner part of the magnetosphere from the convection electric field [e.g., *Wolf et al.*, 2007]. This shielding mechanism can break down during large geomagnetic storms, which allows the large-scale electric field to move farther earthward and sweep away the outer plasmasphere. In the less-dense region outside the plasmasphere, chorus waves can accelerate electrons to radiation belt energies [e.g., *Horne et al.*, 2005], so this inward motion of the plasmapause allows energetic electron populations to form closer to Earth. The coupling between different plasma populations in the magnetosphere highlights the importance of understanding the structure of the quasi-static electric field.

The large-scale dawn-dusk electric field in the inner magnetosphere was previously studied in relation to the *Kp* geomagnetic index using data from the Combined Release and Radiation Effects Satellite (CRRES) [*Rowland and Wygant*, 1998]. The CRRES mission was launched on 25 July 1990 into an 18° inclination orbit with apogee near geosynchronous and perigee of 300 km. Two key results of this study were that a broad local maximum in the dawn-dusk electric field occurred between $L = 3$–6 for moderate *Kp* (4–5), and for the highest geomagnetic activity levels ($Kp > 7$), strong electric fields were observed inside $L = 3$. The observed electric fields below $L = 3$ for high *Kp* values were not expected based on the conventional model at the time [*Volland*, 1973; *Stern*, 1977], which assumed that the electric field was shielded near Earth, and the CRRES

results also show that the quasi-static electric field is much more dynamic than a simple superposition of convection and corotation suggests.

The *Rowland and Wygant* [1998] CRRES-based study does not constitute the only prior observational evidence of strong electric fields on subauroral field lines in the dusk-midnight sector. The earliest evidence was ionospheric rather than magnetospheric. Since strong magnetic field-aligned electric fields are unlikely to exist on subauroral field lines, those field lines are normally assumed to be approximate equipotentials, which means that the equatorial potential pattern can be mapped to the ionosphere and vice versa. In the quasi-dipolar subauroral region, a radially outward electric field in the equatorial plane maps to a poleward electric field in the ionosphere. Narrow ($<1°$), intense regions of poleward electric field discovered in the topside ionosphere many years ago [*Galperin et al*., 1974; *Smiddy et al*., 1977; *Spiro et al*., 1979] were called "polarization jets" or "SubAuroral Ionization Drift" (SAID) events. SAID events were mainly associated with the late stages of substorms. Later *Yeh et al*. [1991] used data from the Millstone Hill incoherent-backscatter radar and the ion drift meter on a DMSP polar orbiter during a major magnetic storm to demonstrate the existence of a several degree wide peak in the poleward ionospheric electric field in the dusk-midnight sector. After the *Rowland and Wygant* [1998] paper, *Burke et al*. [1998] found that SubAuroral Polarization Streams (SAPS) flows observed by DMSP at low altitudes during a major storm lay on approximately the same field lines as strong flows observed by CRRES near the equatorial plane. Later, *Foster and Vo* [2002] used Millstone Hill data for a detailed statistical study of the strong flow events that occur in major storms and cover a wider range of latitude than SAID events, which are primarily associated with substorms. The storm-associated events were called SubAuroral Polarization Streams (SAPS). The *Foster and Vo* [2002] study covered a wide range of local time (14 LT to 06 LT).

On the theoretical side, *Southwood and Wolf* [1978] proposed an explanation for SAID events by showing how a region of strong poleward ionospheric electric field (antiearthward in equatorial plane) is the natural result of the inner edge of plasma sheet ions, which are primarily responsible for shielding the inner magnetosphere, penetrating farther earthward than plasma sheet electrons, which are primarily responsible for enhancing ionospheric conductance. The result is that part of the shielding field-aligned current flows into a low-conductance subauroral region of the ionosphere. Completion of the circuit requires an intense electric field across a low-conductance band between the equatorward edge of the shielding current and the equatorward edge of the diffuse aurora. There is no apparent need for a corresponding intense electric field on the dawnside because the plasma sheet electrons there generally penetrate closer to Earth than most plasma sheet ions. Once the Rice Convection Model developed to the point of treating plasma sheet electrons and ions separately, simulations of substorm conditions [*Harel et al*., 1981] showed a similar feature. Later simulations [*Garner et al*., 2004; *Sazykin et al*., 2005] showed similar features at slightly lower latitudes and covered a wider latitudinal range during magnetic storms, and those features bore a strong resemblance to SubAuroral Polarization Stream (SAPS) events.

More recently, an empirical electric field model was developed by *Matsui et al*. [2008] based on data from Cluster. Due to the polar orbit of the Cluster spacecraft, magnetospheric electric field observations are mostly measured at high magnetic latitudes and are then mapped to the equator using a magnetic field model. Additionally, the perigee of Cluster is 4 R_E, so the region below $L = 4$ cannot be sampled. The low-inclination Time History of Events and Macroscale Interactions during Substorms (THEMIS) spacecraft allow the equatorial electric field to be measured in situ between 1.5 and 12 R_E, offering a unique view of the inner magnetospheric electric field that is complimentary to the Cluster data.

CRRES provided highly accurate (<0.1 mV/m) near-equatorial electric field measurements; however, the mission was limited to only 15 months due to an on-orbit anomaly. This caused the data to be biased in local time, with most of the measurements occurring on the duskside. The question must be raised whether the results of electric field variation with L are duskside features, or if they are applicable to all local times. We address this issue using double-probe electric field data from the Time History of Events and Macroscale Interactions during Substorms (THEMIS) mission [*Angelopoulos et al*., 2008], which covers all local times and radial distances in the inner magnetosphere for over 6 years.

This study follows the methodology of the previous CRRES study [*Rowland and Wygant*, 1998] by sorting the electric field data by *Kp* to investigate the radial profile of the dawn-dusk electric field and offers new insights into the local time dependence based on the extensive THEMIS data set. CRRES offered an order of

magnitude more in situ equatorial electric field data in the inner magnetosphere than had been previously published, and THEMIS provides another order of magnitude more data than CRRES.

2. Instrumentation

The five identical THEMIS probes were launched on 17 February 2007 with inclinations $<10°$. The orbit apogees range from 10 to 30 R_E, and the perigees are near 1.5 R_E, allowing for in situ measurements of the near-equatorial electric field over the entire inner magnetosphere. In 2010, two of the probes were moved to a lunar orbit as part of the Acceleration, Reconnection, Turbulence and Electrodynamics of the Moon's Interaction with the Sun mission, but the other three probes continue to offer data from the magnetosphere. This study focuses on data from THEMIS Probes A, D, and E, which have apogees of approximately 12 R_E, over the time period from 1 January 2009 and 31 December 2012.

Each THEMIS spacecraft is equipped with an Electric Field Instrument (EFI) [*Bonnell et al*., 2008] that provides low-frequency electric field measurements in the spin plane, as well as three-axis wave measurements. The spin period of each spacecraft is approximately 3 s, with the spin axis roughly aligned with the ecliptic normal. Electric fields are inferred using the double-probe technique, which compares the potential difference between opposite sensors separated by a large distance from the spacecraft. The spin-plane booms provide 40 and 50 m separation in orthogonal directions, and the axial sensors are 6.9 m apart. Due to the close proximity of the axial sensors to the spacecraft, the low-frequency axial measurement is often contaminated and is generally not considered to be reliable; however, using the frozen-in assumption, the axial component of the electric field can be inferred when the local magnetic field vector is sufficiently out of the spin plane [*Bonnell et al*., 2008].

For the purposes of this study, we only use electric fields that are directly observed by the spin-plane booms, focusing on the MGSE (Modified Geocentric Solar Ecliptic) *Y* component. This coordinate system has the *Z* axis aligned with the spacecraft spin axis, and the *X* axis is chosen such that the Sun is in the *X-Z* plane. The Y_{MGSE} measurement roughly corresponds to the dawn-dusk electric field in the inner magnetosphere. Using the Y_{MGSE} measurement exclusively also eliminates the complexity of removing sunward offsets due to probe shadowing and photoelectron coupling between the probes and the spacecraft, which are common sources of error for double-probe instruments [e.g., *Pedersen et al*., 1998].

Electrostatic wakes are also known to introduce spurious electric fields in double-probe measurements [*Eriksson et al*., 2006]. Wakes are formed when the ion flow velocity is greater than the ion thermal velocity, which causes an ion depletion behind the spacecraft because the incoming ions are blocked by the spacecraft and their thermal velocity is too slow to fill the region. However, the electrons have much higher thermal velocity than the ions and are able to penetrate the wake, resulting in a charge asymmetry and an apparent electric field. As will be shown in section 4, the THEMIS data strongly agree with the CRRES results where coverage from the two missions overlaps. The CRRES booms were much longer (~90 m separation) than the THEMIS booms (~50 m separation), so the wake was not a significant factor for CRRES. Due to the agreement with CRRES, we believe that wakes have a minimal impact on the long-term average electric field measurement by THEMIS, and we have not attempted to identify or remove wakes from the data.

The THEMIS EFI measurements have a scale factor uncertainty, known as boom shorting, that causes the measured electric field to be smaller than the true electric field due to coupling between the spacecraft and the probes [*Pedersen et al*., 1998]. Boom shorting has been estimated to introduce an approximately 30% reduction in the measured electric field by comparing $-\mathbf{v_i} \times \mathbf{B}$ ($\mathbf{v_i}$: ion velocity vector, $\mathbf{B}$: measured magnetic field vector) from the electrostatic analyzer and the fluxgate magnetometer to the double-probe measurement in the magnetosheath [*Bonnell et al*., 2008]. However, this factor changes as the spacecraft traverses varying plasma environments in the magnetosphere, potentially introducing significant errors near Earth where the induced $\mathbf{v_{sc}} \times \mathbf{B}$ ($\mathbf{v_{sc}}$: spacecraft velocity vector) and corotation electric fields, which must be subtracted from the measurement, are much larger than the variations in the dawn-dusk electric field that we are attempting to extract. For the purposes of this study, we have assumed no boom-shorting effects in order to minimize the impact of the induced and corotation subtraction errors inside the plasmasphere. This may cause the reported electric field to be smaller than the true field for larger L shells but does not significantly impact on the overall trends with geomagnetic activity. The significance of the shorting factor will be discussed in more detail in Appendix A.

3. Data Processing

This study includes all valid data from THEMIS Probes A, D, and E between 1 January 2009 and 31 December 2012. On board spin-fit electric field data are used, which are sampled at the spacecraft spin period (~3 s). The probes rely on photoemission to properly couple to the plasma, so all eclipse periods are removed. Also, large electric field outliers and intervals when the spacecraft potential was outside of the typical range are excluded by visual inspection. The spacecraft potential is usually ~1–2 V near perigee, and it increases to 30–50 V in more tenuous plasmas farther from Earth.

The electric field data are expressed in the frame corotating with Earth, so we compute and subtract both the induced $\mathbf{v_{sc}} \times \mathbf{B}$ due to the motion of the spacecraft with respect to Earth's magnetic field and the corotation electric field using spacecraft ephemeris data and on board fluxgate magnetometer measurements [*Auster et al*., 2008]. Next, the data are averaged in 5 min intervals to filter waves that are not removed by spin averaging. Low-frequency waves with periods greater than 5 min are known to be common in the inner magnetosphere [e.g., *Dai et al*., 2013], but these waves are sufficiently averaged out by spatial binning and the long time interval of the data set to accurately represent the average quasi-static component of the electric field. For the radial profile of the electric field, the data are binned by L shell in 1 R_E intervals for a given local time sector. The local time sectors are defined as dusk (15:00 < MLT <21:00), midnight (21:00 < MLT <03:00), dawn (03:00 < MLT <09:00), and noon (09:00 < MLT <15:00). The *L* value is computed as the radial distance of the field line at the magnetic equator using spacecraft position and assuming a dipole approximation of the Earth's magnetic field.

A significant amount of effort was expended investigating the details of the spin-fit data and the various systematic biases in the measurement prior to compiling the data for this study. We reviewed the impact of probe shadowing spikes when the Sun is close to the spin plane on the spin-fit data and studied the sunward and antisunward offsets that occur inside and outside of the plasmasphere [*Califf et al*., 2013]. The varying offsets in the sunward component of the measurement present significant challenges for a large-scale statistical study of this kind; and therefore, we have focused only on the dawn-dusk component of the electric field. By comparing the on board spin-fit estimate of the dawn-dusk electric field to the spin-resolution measurement when the spin-plane booms were aligned with Y_{MGSE}, we determined that the slow-survey spin-fit data very closely match the direct dawn-dusk measurement, even when significant offsets are present in the sunward direction. This allows us to use slow-survey data, which are available over the entire orbit.

4. Results and Discussion

Figure 1 presents a comparison of the radial profile of the average dawn-dusk electric field based on the CRRES and THEMIS data as a function of the *Kp* index. The CRRES data were limited to MLT between 12:00 and 04:00, while the THEMIS plot represents MLT from 16:00 to 23:00. The THEMIS local time interval was chosen to approximately match the local times where CRRES had full radial coverage in order to make a meaningful comparison of the observations over the full range of L shells. Each plot shows the mean of the data in a given *Kp* and L shell bin, and the error bars represent the variance of the mean following the original CRRES study [*Rowland and Wygant*, 1998]. The error bars are generally smaller than the width of the line used to plot the trends, which reflects an accurate determination of the mean of the sampled data due to the large number of observations included in the study (4 years of 5 min averaged data from three spacecraft). Although the mean values are well defined, there is significant variation in any given observation. The standard deviations of the data in each bin are generally on the order of 1–2 mV/m, and increasing variation is observed with higher *Kp*.

Qualitatively, the data convey remarkable similarities in the observed structure of the quasi-static electric field as the level of geomagnetic activity increases. The dawn-dusk electric field magnitude generally increases with *Kp*, and a broad local maximum develops for moderate activity levels between $L = 4$ and 5. There were relatively few large geomagnetic storms from 2009 to 2012, so there are not many data points for the THEMIS results above $Kp = 6$. However, strong electric fields were observed inside $L = 3$ during the most active times, which is consistent with the CRRES observations. Additionally, the dawn-dusk electric field is shielded close to Earth for low *Kp*, as indicated by the approach to zero magnitude as *L* decreases.

It should be noted that the absolute magnitude of the results below $L = 4$ may be affected by uncertainties in the induced and corotation electric field subtraction related to the variable boom-shorting factor for THEMIS,

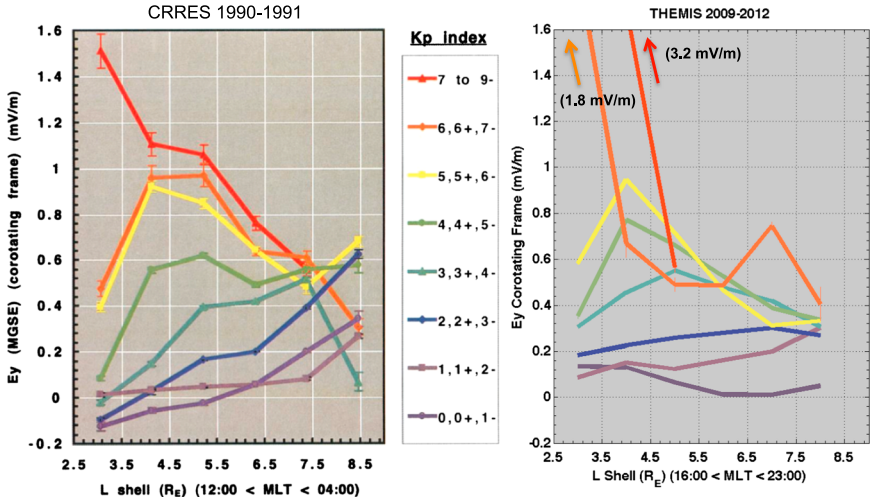

Figure 1. Dawn-dusk electric field in the frame corotating with Earth as a function of the *Kp* index. The data are binned in 1 R_E intervals, with the mean of the data plotted at the center of the L shell bin. The error bars represent the variance of the mean. (left) Results from the CRRES mission for MLT between 12:00 and 04:00 (Plate 1) [*Rowland and Wygant*, 1998]. (right) THEMIS observations from 2009 to 2012 using probes A, D, and E for MLT between 16:00 and 23:00.

although the relative increase in magnitude with *Kp* should be independent of this effect. Also, a direct comparison between CRRES and THEMIS measurements for higher L shells could be impacted by the different magnetic latitudes at which the electric fields were measured. CRRES was in a geotransfer orbit, so L shells above 6.6 R_E could only be sampled at latitudes off of the magnetic equator. This has the effect of amplifying the electric field because the magnetic field lines are considered to be equipotentials, and they converge at higher-magnetic latitudes [*Mozer*, 1970]. The THEMIS data are also somewhat affected by sampling off the magnetic equator, but with apogees near 12 R_E, the larger L shells can be accessed at lower magnetic latitudes.

The main advantage of the THEMIS data set is full local time coverage, which enables us to explore the local time dependence of the dawn-dusk electric field. Figure 2 shows the results divided into four local time sectors: dusk (15:00 < MLT <21:00), midnight (21:00 < MLT <03:00), dawn (03:00 < MLT <09:00), and noon (09:00 < MLT <15:00). The data have been restricted to *Kp* <6 to highlight the trends in bins where there are a significant number of samples. For *Kp* >6, there are relatively few samples (~30 orbits) and the average magnitudes are much larger (up to 3 mV/m) than for less active times, which tends to overwhelm the local time dependency seen in the *Kp* <6 bins. The strongest electric fields are observed on the duskside, with the average magnitudes being approximately a factor of 2 greater than the other local time sectors, even during quiet times.

The enhanced electric field region between dusk and midnight has been attributed to subauroral polarization streams (SAPS). SAPS are strong poleward electric fields generated by field-aligned currents that close through the low-conductivity region of ionosphere and then map back out the equatorial magnetosphere along magnetic field lines [e.g., *Foster and Vo*, 2002]. DMSP ion drift-meter data and Millstone Hill radar data from specific events often show two or more peaks in the poleward electric field, plotted as a function of latitude in the dusk sector [e.g., *Foster and Vo*, 2002, Figure 2; *Foster et al.*, 2014, Figure 1c]. However, multiple peaks are not prominent in Figure 2. The dual-peak structure is likely smoothed out by the broad-binned statistical averages used in this study, and it is possible that the high-latitude peak maps out to beyond 8 R_E and would not be present in our results.

Generally, the trends for dusk, dawn, and midnight are similar, with the local maximum observed near $L = 4$ for moderate *Kp* and strong electric fields observed close to Earth in the higher *Kp* bins. It is especially important to note that the in the midnight sector, there is no clear enhanced dawn-dusk electric field at higher L shells for increased *Kp*. The *Kp* index is generally associated with increased magnetospheric convection, so one would expect that as *Kp* increases, there would be stronger earthward flows from the magnetotail that would cause an increase in *Ey* at higher L shells near midnight. These results are a striking illustration of how the electric field in the inner magnetosphere is significantly affected by coupling with the ionosphere, and not purely determined by enhanced earthward convection from the magnetotail that extends close to Earth.

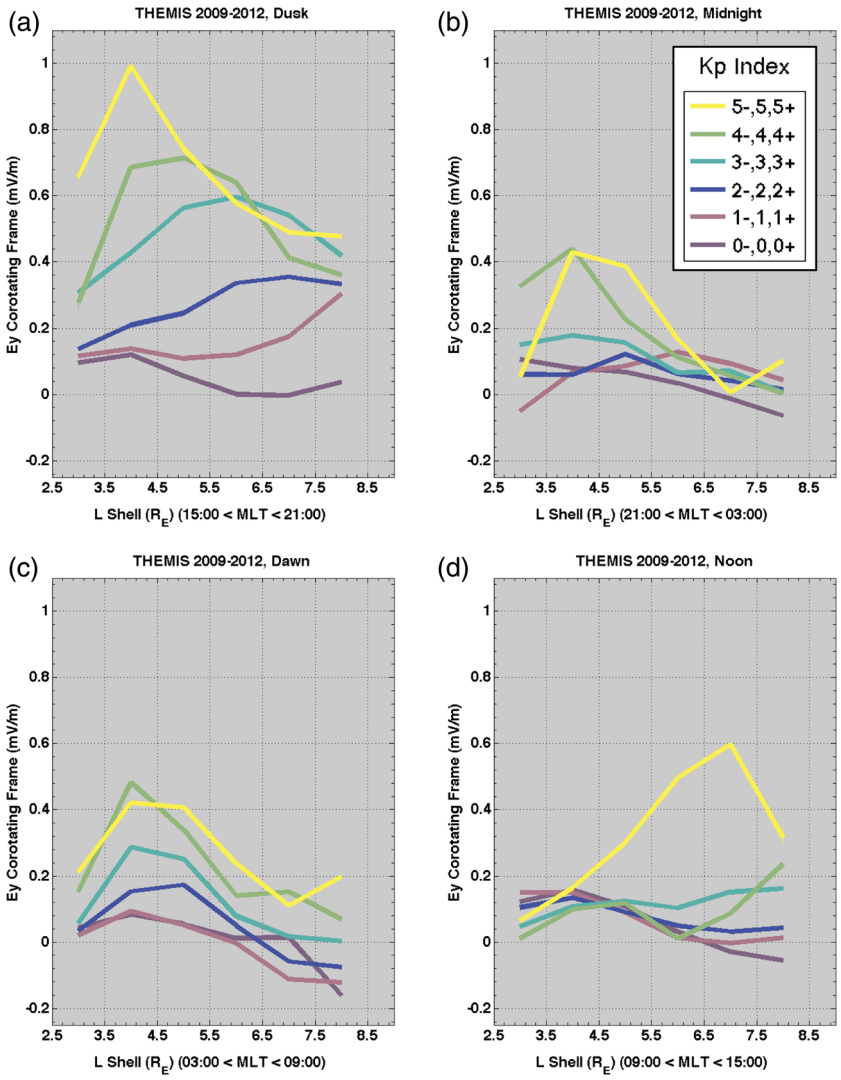

Figure 2. Radial profiles of the dawn-dusk electric field in the frame corotating with Earth as a function of the *Kp* index for the (a) dusk, (b) midnight, (c) dawn, and (d) noon local time sectors. Data are only shown for $Kp < 6$.

In the noon sector, the average electric field is almost exclusively below 0.2 mV/m when $Kp < 5$, and while stronger electric fields are observed for higher *Kp*, the peak is located near $L = 7$ rather than $L = 4$ as in the other local time sectors. We suspected that these enhanced electric fields may have been related to dayside magnetopause crossings; however, only one magnetopause crossing was clearly identified (and subsequently removed from the data set) for the *Kp* 5–6 bin in the noon sector inside $L = 8.5$, and there were ~1 mV/m dawn-dusk electric fields between $L = 7$ and 8 leading up to the crossing. While it is possible that the statistics are skewed by some measurements outside of the magnetopause, there is still strong evidence of enhanced electric fields near $L = 7$ inside the magnetosphere for $Kp > 5$. There is evidence that the SAPS flow moves to higher latitude (at ionospheric heights) near local noon, and its equatorial projection (the plasmaspheric plume, which is the plasma carried by the SAPS) moves toward the dayside magnetopause [*Walsh et al.*, 2014]. The increased *Ey* magnitude seen by THEMIS at $L \sim 7$ near local noon may be due to crossing the SAPS and plume in this local time sector.

Synoptic maps of the data for CRRES and THEMIS are displayed in Figure 3, with color representing the magnitude of the dawn-dusk electric field in the frame corotating with Earth. The L shell and MLT corresponding to each electric field measurement were converted to Cartesian coordinates and then were averaged in 0.5 $R_E \times 0.5$ R_E bins. For $Kp < 3$, there were over 35,000 h of THEMIS data, and the *Kp* 3–6 bin was

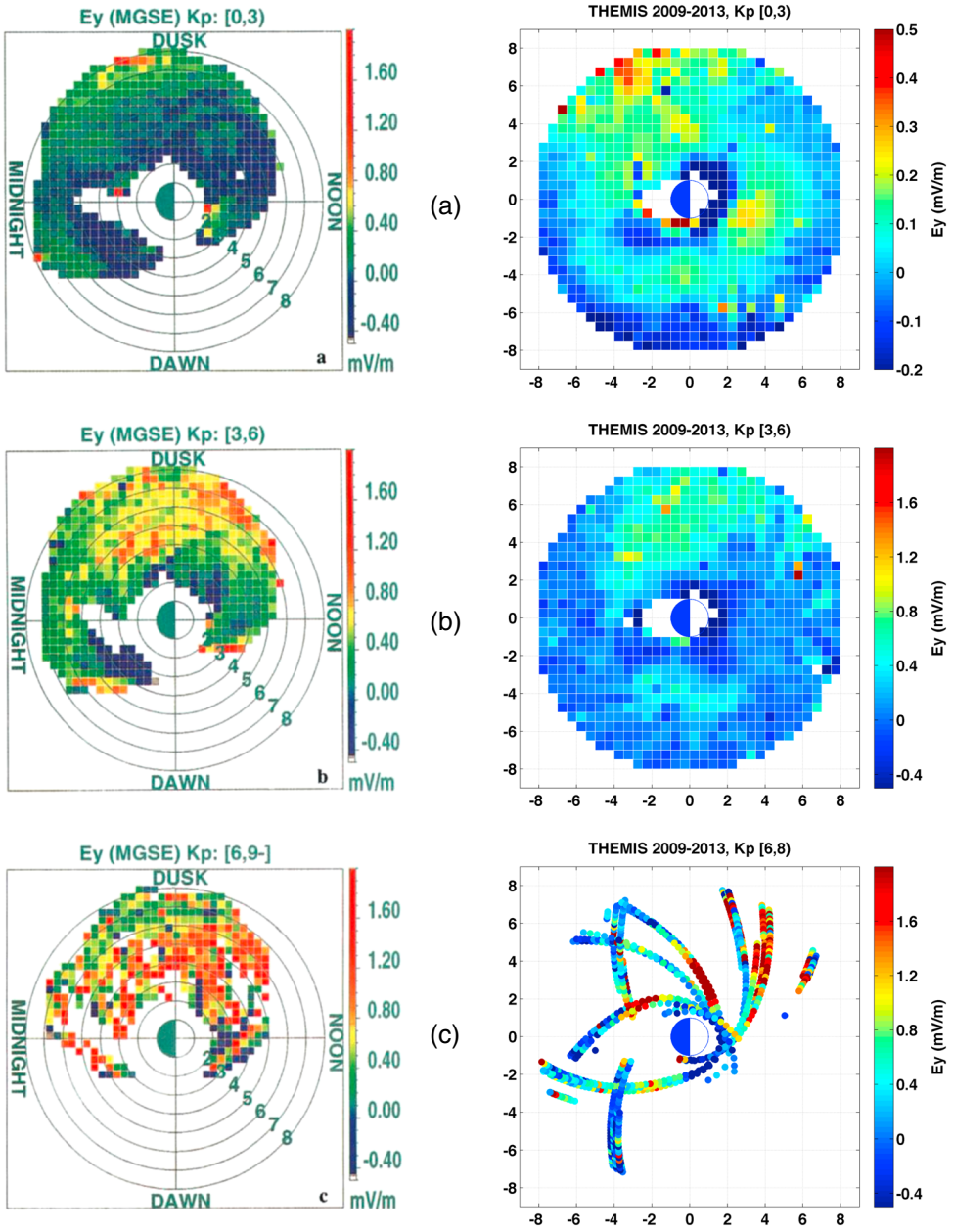

Figure 3. Synoptic maps of the dawn-dusk electric field in the frame corotating with Earth observed by (left) CRRES (Plate 2) [*Rowland and Wygant*, 1998] and (right) THEMIS for varying levels of geomagnetic activity: (a) $0 \leq Kp < 3$, (b) $3 \leq Kp < 6$, and (c) $6 \leq Kp < 9$. The data shown are polar plots of *L* and MLT with the *Ey* magnitude represented in color. Each plot contains spatially binned averages except Figure 3c, right, which shows 5 min averages of the electric field from various THEMIS orbits overlaying each other to better convey the data coverage.

well sampled with 368 days of unique observations comprising over 4000 h of coverage. However, there were only 12 days of data with $Kp > 6-$, which coincidentally resulted in most of the sampling occurring on the duskside during the most active times. It should be noted that the color scales for the CRRES data are held constant, while the color range for THEMIS in Figure 3a is smaller in order to accentuate the spatial variation in the electric field during periods of low-geomagnetic activity.

Overall, there is excellent agreement in the structure of the large-scale electric field between CRRES and THEMIS for the regions of the magnetosphere covered by both missions. During low *Kp* intervals ($0 \leq Kp < 3$), the strongest electric fields are in the dusk-midnight sector, with a similar enhancement observed by THEMIS

and CRRES near $L = 7$ just after dusk. The THEMIS results also show electric fields on the order of 0.1–0.2 mV/m spanning $L = 3$–6 from dawn through noon that was outside of the CRRES coverage, as well as confirmation of a localized enhancement near 11:00 MLT at $L = 3$ that was present in the CRRES data.

During periods of moderate geomagnetic activity (*Kp* 3–6), there are enhanced electric fields on the duskside, concentrated between 18:00 and 24:00 MLT. The day-night asymmetry of the radial dependence of *Ey* on the duskside was noted based on the CRRES results [*Rowland and Wygant*, 1998], although it was unclear whether this was real, or that it was caused by an increased occurrence of geomagnetic storms during certain phases of the CRRES orbit precession. Based on 4 years of THEMIS data, we confirm that this asymmetry is a physical feature, with the enhanced region on the duskside extending as close as $L = 3$–4 near 21:00 MLT, but being confined to beyond $L = 6$ by 15:00 MLT. The THEMIS data also reveal a local enhancement of ~0.4 mV/m on the dawnside centered near $L = 4$ that is outside of the CRRES coverage.

We should remark that *Huang et al*. [2001] reported on the latitude variations of convective flow observed from Millstone. Their observations were for one major storm and one minor one. For those events, they found a range of local times extending from before midnight to past dawn (in one case) where there was systematic eastward flow at auroral latitudes, but strong westward flow at subauroral latitudes. Their results show the peak of the westward flow at subauroral latitudes occurring at lower latitudes near midnight, and moving to higher latitudes toward dusk, which is in agreement with the duskside features observed by CRRES and THEMIS. On the dawnside, the westward flow reported by *Huang et al*. [2001] corresponds to $Ey < 0$ in the equatorial plane, in contradiction to the statistical averages shown in Figure 2b. We do not have a compelling explanation for the difference in the two results. Of course, the studies were quite different (e.g., two events versus statistical average).

A qualitatively similar, locally enhanced dawn-dusk electric field on the dawnside near $L = 4$ has been observed in a self-consistent magnetospheric electric field model by *Gamayunov et al*. [2009]. The model specifies the electric potential at high- and low-latitude boundaries, and then computes the ionospheric potential based on ring current pressure, field-aligned currents, and ionospheric conductivity. The magnetospheric electric field is derived by mapping the ionospheric potential back out to the magnetosphere. Although dawn-dusk electric field maxima at lower L shells on both the dawn and dusksides are qualitatively reproduced by the model, the predicted magnitudes are much larger than the electric fields observed by CRRES and THEMIS. Rice Convection Model simulations by *Garner et al*. [2004] also reproduce a dawnside local *Ey* enhancement near $L = 4$ but show an additional negative *Ey* peak on the dawnside at lower L shells that is not apparent in the THEMIS statistical data. The positive *Ey* peak near $L = 4$ and the negative *Ey* peak at lower L are also seen in Comprehensive Ring Current Model runs by *Fok et al*. [2003]. The model results discussed here are from individual runs for specific storms, and given the many factors involved in determining the inner magnetospheric electric field, it is not surprising that there are discrepancies between the models and the statistical averages presented in this paper.

For the THEMIS results with $Kp > 6$ (Figure 3c, right), the raw 5 min averages are displayed rather than the binned data to convey the relatively few number of orbits that occurred during periods of high geomagnetic activity. Despite the sparse data coverage, there is clear evidence that the strong electric fields occur close to Earth during very active times. The enhancement also appears to be greater on the duskside, although much of the dawnside has not been sampled by either mission for $Kp > 6$. The few THEMIS orbits on the dawnside in Figure 3c consistently show electric fields below 0.5 mV/m, but there are many observations with magnitudes greater than 1.5 mV/m on the duskside. The THEMIS data also highlight the spatial variability of the electric field during active times. For instance, multiple orbits passed through the predusk sector during different time periods with $Kp > 6$, and some observed electric fields greater than 1.5 mV/m, while others report dawn-dusk electric fields near 0 mV/m in nearly the same spatial location. For $Kp < 6$, electric field enhancements were observed in very specific locations, but the strong electric fields during the most active times appear to be less predictable, although they are generally concentrated on the duskside.

The dawn-dusk electric field is expected to be mostly positive and is associated with sunward convection from the magnetotail. However, both CRRES and THEMIS observed small average dusk-dawn electric fields in some regions of the inner magnetosphere, possibly indicating antisunward convection. Some of these negative electric fields can be attributed to induced and corotation electric field subtraction errors in locations close to Earth, but there appears to be a region of slightly negative electric field extending across

the entire dayside for $L < 2$ for all *Kp* values that may be real. This feature cannot be explained simply by a systematic $v \times B$ subtraction error because the induced electric field is positive on the duskside and negative on the dawnside. Also, the small negative fields near $L = 7$ across the dawnside are on the same order as the magnitude of the corotation electric field in this region. These observations could indicate average stagnant flow, rather than the apparent antisunward convection that arises from subtracting the expected corotation electric field.

The extensive data set from THEMIS offers important new insights into the structure of the quasi-static electric field as the geomagnetic activity level changes, as this is the first study to provide complete local time coverage based on in situ equatorial measurements. First, the revolutionary results first reported by CRRES are confirmed, showing that the electric field is enhanced near Earth during moderately to highly active times. This behavior is consistent in the dusk, midnight, and dawn sectors, although the magnitudes are greater on the duskside. Near local noon, we observed behavior more consistent with the conventional model of an externally imposed large-scale convection electric field that is shielded near Earth, although the enhancement at higher L shells near noon may be related to SAPS moving to higher latitudes and convecting the plasmaspheric plume toward the dayside magnetopause. Also, the ambiguity of the day/night asymmetry in the CRRES results has been resolved, with enhancements occurring closer to Earth in the dusk-midnight sector and at larger radial distances in the predusk sector. The dawnside enhancement near $L = 4$ for moderate to high *Kp* is a new magnetospheric observation made by THEMIS, as CRRES did not sample the dawnside. This feature is commonly explained by SAPS on the duskside; however, SAPS are not thought to be prevalent beyond 03:00 MLT [*Foster and Burke*, 2002]. Additionally, a poleward SAPS electric field would produce a negative *Ey* on the dawnside, which is in the opposite direction to the THEMIS statistical observations.

5. Summary

The quasi-static electric field in the inner magnetosphere is much more spatially dynamic than the basic model of convection and corotation suggests. Previous observations by CRRES offered the first in-depth view of the structure of the large-scale electric field using in situ measurements near the equatorial plane. The results showed that the dawn-dusk electric field is shielded near Earth for low *Kp*, and that there is a local maximum near $L = 4$ during periods of moderate geomagnetic activity. Also, strong electric fields were observed near $L = 3$ during the most active times. However, the CRRES measurements were limited to the duskside, motivating our effort to cover all local times using THEMIS.

Observations from THEMIS confirmed the CRRES results on the duskside, and, for the first time, provided a detailed view of the quasi-static electric field across the entire inner magnetosphere using in situ equatorial measurements. These results revealed a strong local time dependence of the structure of the electric field. The largest electric fields were located on the duskside, with a maximum appearing closest to Earth near 21:00 MLT. On the dawnside, there was a similar peak in dawn-dusk electric field at $L = 4$, but overall, the magnitudes were about a factor of 2 smaller than on the duskside. The smallest average electric fields were observed in the noon sector, and as *Kp* increased, the peak was found to be located farther out, near the dayside magnetopause, in contrast to the enhancement near $L = 4$ for the other local time sectors.

These results using the full local time coverage of THEMIS are important to understanding the dynamics of plasma in the Earth's magnetosphere and the coupling between the ionosphere and the magnetosphere. Previously, this type of complete picture of the electric field has only been available by mapping high-latitude ionospheric measurements to the equatorial magnetosphere using magnetic field models. Also, the somewhat controversial CRRES results of enhanced electric fields near Earth have been strongly confirmed, with the additional detail that the behavior is not observed near local noon. Finally, the local maximum in *Ey* on the dawnside near $L = 4$ during periods of moderate geomagnetic activity is a new observation that was not covered in the CRRES data.

Appendix A: Boom-Shorting Considerations

One potential source of systematic bias in the THEMIS data is the variable boom-shorting factor combined with large induced and corotation electric fields near Earth that must be subtracted from the measurement. Boom shorting is related to coupling between the spacecraft and the probes, and has the effect of reducing the magnitude of the measured electric field. The shorting effect is minimal when the local Debye length is

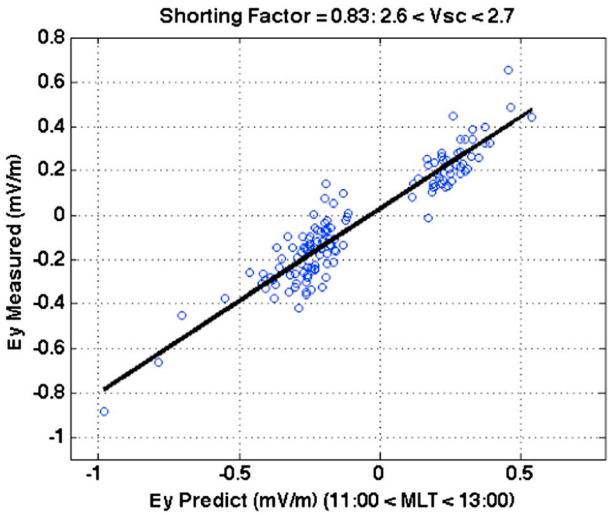

Figure A1. Example of the shorting factor estimate for spacecraft potential between 2.6 and 2.7 V. The measured electric field is plotted against the sum of the calculated induced $\mathbf{v_{sc}} \times \mathbf{B}$ and the corotation electric fields, and the slope of the linear fit indicates a shorting factor of 0.83.

much smaller than the length of the wire booms because the ambient plasma shields the probes from the spacecraft, allowing for independent measurements of potential differences in the plasma. If the Debye length is equivalent or greater than the length of the booms, an effective short circuit develops between the spacecraft and the probes [*Pedersen et al*., 1998]. Near perigee, the THEMIS spacecraft are deep inside the plasmasphere where densities are high, and the corresponding Debye length ($<$1 m) is small relative to the boom length (25 m from the spacecraft to the spherical sensor). As the spacecraft move out of the plasmasphere, the density decreases dramatically and the Debye length increases to be on the order of the boom length or greater, causing an increase in the shorting effect. Based on calibrations in the magnetosheath [*Bonnell et al*., 2008], we expect the shorting factor to be close to 0.7 (30% reduction in measurement) outside of the plasmasphere, but inside the plasmasphere, where the density is high, the shorting factor should be approximately 1.0 (no shorting effect). Note that boom shorting was not a driving consideration for the CRRES measurements because the wire booms were approximately a factor of 2 longer than the THEMIS booms, causing coupling effects between the probes and spacecraft to be less significant.

In addition to measuring electric fields, the double-probe instrument provides an estimate of spacecraft potential by taking the average of the negative measured potentials from opposite spheres. Spacecraft potential is inversely related to plasma density, as the spacecraft charges more positively in a low-density plasma because current from escaping photoelectrons dominates the current due to incoming ambient electrons. We use spacecraft potential as a proxy for Debye length and attempt to estimate the shorting factor as a function of spacecraft potential in order to evaluate the impact of this uncertainty on the results.

The shorting factor can be calibrated in regions absent of large currents or pressure gradients by comparing the double-probe measurement to the calculated frozen-in electric field based on the measured ion velocity and magnetic field ($\mathbf{E} = -\mathbf{v_i} \times \mathbf{B}$). However, there are calibration issues with the electrostatic analyzer on THEMIS that make a comprehensive comparison of the double-probe measurements and the ion moments outside of the scope of this work. Instead, we have chosen data during geomagnetically quiet times and performed a calibration assuming that the long-term average electric field is determined by corotation only. The quiet-time criteria used are that $Kp < 2-$ for three consecutive days, and each selected data point has $Kp < 1-$. Because we are interested the dawn-dusk component, the data are limited to near local noon (11:00 $<$ MLT $<$13:00), which places the radially inward pointing corotation electric field roughly orthogonal to the measurement. This minimizes the impact of the assumption that the plasmasphere is perfectly corotating, as observations have shown that the plasmasphere lags behind Earth's rotation by 10–15% near 2–3 R_E [*Burch et al*., 2004]. Close to Earth, the signal is dominated by the induced electric field due to spacecraft motion, which is well known based on spacecraft ephemeris data and the on board magnetometer measurements. The shorting factor is then estimated by performing a linear fit of the measurements to the predicted induced and corotation electric fields.

An example of the shorting factor estimate is shown in Figure A1 for spacecraft potential between 2.6 and 2.7 V. The predicted electric field is the sum of the calculated induced $\mathbf{v_{sc}} \times \mathbf{B}$ electric field due to spacecraft motion in the Earth's magnetic field and the corotation electric field $-(\boldsymbol{\omega_E} \times \mathbf{R}) \times \mathbf{B}$ ($\boldsymbol{\omega_E}$: Earth's angular rate vector, $\mathbf{R}$: spacecraft position vector) assuming the plasma is perfectly corotating with Earth. A linear fit of the measurement to the predicted electric field shows a slope of 0.83, which can be interpreted as the

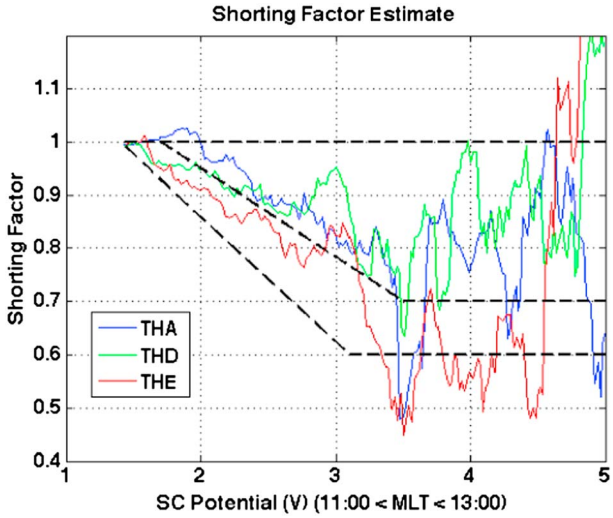

Figure A2. Estimated shorting factor as a function of spacecraft potential for THEMIS A, D, and E (solid lines) based on a comparison of the measured electric field to the calculated induced and corotation electric fields. Also shown are the functions assuming no shorting (top dashed line), the nominal estimate from the data (middle dashed line), and worst-case maximum shorting function (bottom dashed line).

measurement being shorted by 27% for this range of spacecraft potential. By repeating this process for a range of spacecraft potential bins, we generate the shorting factor as a function of spacecraft potential shown in Figure A2. For V_{sc} <3 V, there is a roughly linear relationship between the shorting factor and spacecraft potential, but for V_{sc} >3 V, the estimate is highly variable. Low values of spacecraft potential correspond to higher-plasma densities and closer proximity to Earth, which is also where the induced and corotation electric fields dominate the measurement. In this region, the measurement and the prediction are well correlated and the estimation technique is more reliable. For higher spacecraft potential, the predicted electric fields are much smaller, so small variations in the geophysical electric field can dominate the measurement, which leads to the "noisy" correlation at high spacecraft potential in Figure A2.

Based on our quiet-time prediction of the shorting factor, there is an indication that boom shorting is a function of spacecraft potential, and that the factor is close to 1.0 for low spacecraft potential and drops fairly linearly to ~0.7 by V_{sc} = 3.5 V. Recognizing the uncertainty in our estimation technique, we have assigned conservative outer limits of where this function may exist (indicated by the outer dashed lines in Figure A2) and have applied the extremes of this function to the data to quantify the impact on the statistical results.

In Figure A3, the radial profile of the dawn-dusk electric field is presented for the dawn and dusk sectors using three different assumptions for the shorting factor as function of spacecraft potential: the nominal shorting

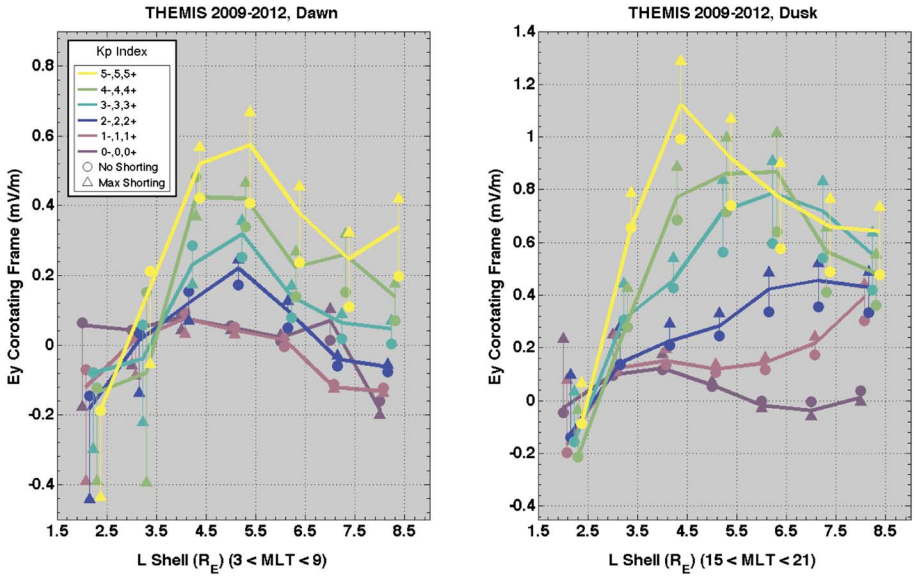

Figure A3. Impact of the boom-shorting factor assumption on dawn and dusk radial profiles of *Ey* (MGSE) in the frame corotating with Earth for the (left) dawn and (right) dusk sectors. The lines are 1 R_E binned averages using the nominal estimated shorting factor as a function of spacecraft potential (middle dashed line, Figure A2), and the error bars show the difference between assuming maximum shorting (bottom dashed line, Figure A2) and no shorting (top dashed line, Figure A2).

factor function indicated by the middle dashed line in Figure A2, maximum shorting, which we estimate to be the worst case, given by the lower dashed line in Figure A2, and no shorting. The thick lines in Figure A3 represent the nominal shorting case, and the maximum shorting (triangle) and no shorting (circle) results are used to create the error bars. The most significant deviations in the average electric field estimate occur inside $L = 4$ and are associated with large induced and corotation electric field subtractions. For higher L values, the maximum shorting function amplifies the magnitudes of the curves but does not qualitatively affect the relative changes in the average electric field as *Kp* increases.

Notice that on the dawnside, the maximum shorting assumption decreases the magnitude of the estimated electric field close to Earth. In this region, the induced electric field dominates the signal and points generally from dawn to dusk ($\mathbf{E} = \mathbf{v_{sc}} \times \mathbf{B}$), so when we assume worst-case shorting on the measurement, we are likely oversubtracting the induced electric field and introducing small, unphysical negative electric fields. The opposite effect occurs at low L on the duskside, where the dominant induced electric field points roughly from dusk to dawn.

We chose a shorting factor of 1.0, or no shorting effect for the results presented in the body of this paper, rather than the nominal shorting function estimated from the data (Figure A2, middle dashed line). Notice that the results assuming no shorting are very similar to those using the nominal estimated shorting function at low L where the induced and corotation subtractions are most significant. However, the maximum shorting case introduces significant deviations in the low L results. This leads us to believe that overestimating the shorting effect near Earth (e.g., assuming a factor of 0.95 when the true factor is 1.0) can introduce more bias than ignoring shorting altogether. At higher L shells, we are likely underestimating the absolute magnitude of the electric field (~20–30%) due to this assumption, but the induced and corotation signals are much weaker farther from Earth, so the effect is primarily a scale factor on the curves rather than an asymmetric dawn-dusk bias.

Acknowledgments

THEMIS data are publicly available at http://themis.ssl.berkeley.edu/, and the *Kp* index can be found at http://omniweb.gsfc.nasa.gov. Work at Rice was supported by NASA grant NNX10AL04G.

Michael Balikhin thanks John Foster and another reviewer for their assistance in evaluating this paper.

References

Angelopoulos, V., et al. (2008), First results from the THEMIS Mission, *Space Sci. Rev.*, *141*, 453–476.

Auster, H. U., et al. (2008), The THEMIS fluxgate magnetometer, *Space Sci. Rev.*, *141*, 235–264.

Bonnell, J. W., F. S. Mozer, G. T. Deloy, A. J. Hull, R. E. Ergun, C. M. Cully, V. Angelopoulos, and P. R. Harvey (2008), The electric field instrument (EFI) for THEMIS, *Space Sci. Rev.*, *141*, 303–341.

Burch, J. L., J. Goldstein, and B. R. Sandel (2004), Cause of plasmasphere corotation lag, *Geophys. Res. Lett.*, *31*, L05802, doi:10.1029/2003GL019164.

Burke, W. J., N. C. Maynard, M. P. Hagan, R. A. Wolf, G. R. Wilson, L. C. Gentile, M. S. Gussenhoven, C. Y. Huang, T. W. Garner, and F. J. Rich (1998), Electrodynamics of the inner magnetosphere observed in the dusk sector by CRRES and DMSP during the magnetic storm of June 4-6, 1991, *J. Geophys. Res.*, *103*, 29,399–29,418, doi:10.1029/98JA02197.

Califf, S., et al. (2013), DC electric field observations from THEMIS and the Van Allen Probes, AGU Poster SM51B-2180.

Dai, L., et al. (2013), Excitation of poloidal standing Alfven waves through drift resonance wave-particle interaction, *Geophys. Res. Lett.*, *40*, 4127–4132, doi:10.1002/grl.50800.

Eriksson, A. I., et al. (2006), Electric field measurements on Cluster: Comparing the double-probe and electron drift techniques, *Ann. Geophys.*, *24*, 275–289.

Fok, M.-C., et al. (2003), Global ENA IMAGE simulations, *Space Sci. Rev.*, *109*, 77–103.

Foster, J. C., and W. J. Burke (2002), SAPS: A new categorization for sub-auroral electric fields, *Eos Trans. AGU*, *83*(36), 393–394, doi:10.1029/2002EO000289.

Foster, J. C., and H. B. Vo (2002), Average characteristics and activity dependence of the subauroral polarization stream, *J. Geophys. Res.*, *107*(A12), 1475, doi:10.1029/2002JA009409.

Foster, J. C., P. J. Erickson, A. J. Coster, S. Thaller, J. Tao, J. R. Wygant, and J. Bonnell (2014), Storm time observations of plasmasphere erosion flux in the magnetosphere and ionosphere, *Geophys. Res. Lett.*, *41*, 762–768, doi:10.1002/2013GL059124.

Galperin, Y. I., V. N. Ponomarev, and A. G. Zosimova (1974), Plasma convection in polar ionosphere, *Ann. Geophys.*, *30*, 1–7.

Garner, T. W., R. A. Wolf, R. W. Spiro, W. J. Burke, B. G. Fejer, S. Sazykin, J. L. Roeder, and M. R. Hairston (2004), Magnetospheric electric fields and plasma sheet injection to low L-shells during the 4–5 June 1991 magnetic storm: Comparison between the Rice Convection Model and observations, *J. Geophys. Res.*, *109*, A02214, doi:10.1029/2003JA010208.

Gamayunov, K. V., G. V. Khazanov, M. W. Liemohn, M.-C. Fock, and A. J. Ridley (2009), Self-consistent model of magnetospheric electric field, ring current, and electromagnetic ion cyclotron waves: Initial results, *J. Geophys. Res.*, *114*, A03221, doi:10.1029/2008JA013597.

Harel, M., R. A. Wolf, R. W. Spiro, P. H. Reiff, C.-K. Chen, W. J. Burke, F. J. Rich, and M. Smiddy (1981), Quantitative simulation of a magnetospheric substorm 2. Comparison with observations, *J. Geophys. Res.*, *86*, 2242–2260, doi:10.1029/JA086iA04p02242.

Horne, R. B., et al. (2005), Wave acceleration of electrons in the Van Allen radiation belts, *Nature*, *437*, 227–230.

Huang, C. S., J. C. Foster, and J. M. Holt (2001), Westward plasma drift in the midlatitude ionospheric F region in the midnight-dawn sector, *J. Geophys. Res.*, *106*(A12), 30,349–30,362, doi:10.1029/2001JA001110.

Matsui, H., P. A. Puhl-Quinn, V. K. Jordanova, Y. Khotyaintsev, P. A. Lindqvist, and R. B. Torbert (2008), Derivation of inner magnetospheric electric field (UNH-IMEF) model using Cluster data set, *Ann. Geophys.*, *26*, 2887–2898.

Mozer, F. S. (1970), Electric field mapping in the ionosphere at the equatorial plane, *Planet. Space Sci.*, *18*, 259–263.

Pedersen, A., F. Mozer, and G. Gustafsson (1998), Electric field measurements in a tenuous plasma with spherical double probes, in *Measurement Techniques in Space Plasmas Fields*, *Geophys. Monogr. Ser.*, vol. 103, edited by R. F. Pfaff, J. E. Borovsky, and D. T. Young, AGU, Washington, D. C., doi:10.1002/9781118664391.ch1.

Rowland, D. E., and J. R. Wygant (1998), Dependence of the large-scale, inner magnetospheric electric field on geo- magnetic activity, *J. Geophys. Res.*, *103*, 14,959–14,964, doi:10.1029/97JA03524.

Sazykin, S., R. W. Spiro, R. A. Wolf, F. R. Toffoletto, N. Tsyganenko, J. Goldstein, and M. R. Hairston (2005), Modeling inner magnetospheric electric fields: Latest self-consistent results, in *The Inner Magnetosphere: Physics and Modeling*, edited by T. I. Pulkkinen, N. A. Tsyganenko, and R. H. W. Friedel, pp. 263–270, AGU, Washington, D. C.

Smiddy, M., M. C. Kelley, W. Burke, F. Rich, R. Sagalyn, B. Shuman, R. Hays, and S. Lai (1977), Intense poleward-directed electric fields near the ionospheric projection of the plasmapause, *Geophys. Res. Lett.*, *4*, 543–546, doi:10.1029/GL004i011p00543.

Southwood, D. J., and R. A. Wolf (1978), An assessment of the role of precipitation in magnetospheric convection, *J. Geophys. Res.*, *83*, 5227–5232, doi:10.1029/JA083iA11p05227.

Spiro, R. W., R. A. Heelis, and W. B. Hanson (1979), Rapid subauroral ion drifts observed by Atmosphere Explorer C, *Geophys. Res. Lett.*, *6*, 657–660, doi:10.1029/GL006i008p00657.

Stern, D. P. (1977), Large-scale electric fields in the Earth's magnetosphere, *Rev. Geophys.*, *15*, 156–194, doi:10.1029/RG015i002p00156.

Walsh, B. M., J. C. Foster, P. J. Erickson, and D. G. Sibeck (2014), Simultaneous ground- and space-based observations of the plasmaspheric plume and reconnection, *Science*, *343*, 1122–1125.

Wolf, R. A., R. W. Spiro, S. Sazykin, and F. R. Toffoletto (2007), How the Earth's inner magnetosphere works: An evolving picture, *J. Atmos. Sol. Terr. Phys.*, *69*, 288–302.

Volland, H. (1973), A semiempirical model of large-scale magnetospheric electric fields, *J. Geophys. Res.*, *78*, 171–180, doi:10.1029/JA078i001p00171.

Yeh, H.-C., J. C. Foster, F. J. Rich, and W. Swider (1991), Storm time electric field penetration observed at mid-latitude, *J. Geophys. Res.*, *96*(A4), 5707–5721, doi:10.1029/90JA02751.